Relationship between magnetic power spectrum and flare productivity in solar active regions

V.I. Abramenko

Big Bear Solar Observatory, 40386 N. Shore Lane, Big Bear City, CA 92314, USA

ABSTRACT

Power spectra of the line-of-sight magnetograms were calculated for 16 active regions of different flare activity. Data obtained by the Michelson Doppler Imager instrument onboard the Solar and Heliospheric Observatory in high resolution mode were used in this study. For each active region, the daily soft X-ray flare index, A, was calculated. This index characterizes the flare productivity of an active region per day, being equal to 1 when the specific flare productivity is one C1.0 flare per day. The power index, α, of the magnetic power spectrum, $E(k) \sim k^{-\alpha}$, averaged over all analyzed magnetograms for a given active region, was compared with the flare index. It was found that active regions, which produced X-class flares, possessed a steep power spectrum with $\alpha > 2.0$, while flare-quiet active regions with low magnitude of A displayed a Kolmogorov-type spectrum of $\alpha \approx 5/3$. Observational data suggest that the flare index A may be determined from the power index α by $A(\alpha) = 409.5(\alpha - 5/3)^{2.49}$. The magnitude of the power index at the stage of emergence of an active region seems not to be related to the current flaring level of this active region, but rather reflects its future flare productivity, when the the magnetic configuration becomes well-evolved. This finding shows the way to distinguish at the very early stage those solar active regions that are "born bad" and have a potential to produce significant disturbances in the earth magnetosphere.

Subject headings: Sun: magnetic field; turbulence; flares

1. Introduction

Photospheric plasma is thought to be in a state of fully developed turbulence at high magnetic Reynolds number. Magnetic fields, present in plasmas, are contained in thin vertical flux tubes (Spruit 1981; Stenflo & Holzreuter 2002 and references in) that diffuse in

the same way as a scalar field in a turbulent flow (Nakagawa & Priest 1973; Parker 1979; Petrovay & Szakaly 1993). The effect of turbulence on magnetic fields is ambivalent. On one hand, any magnetic field concentration present in a turbulent flow, tends to be smeared out by turbulent diffusion. On the other hand, turbulent motions tend to sweep the field lines together at convergence points of plasma flow (Parker 1979).

In homogeneous stationary MHD turbulence the structure of the magnetic field is essentially determined by a dynamical equilibrium between turbulent diffusion and convergence and a stationary turbulent regime with constant rate of energy transfer along the spectrum is holding. Due to an equilibrium between the input of energy at large scales and the output at small scales, the evolution of a system may proceed without catastrophes.

For turbulent flows without magnetic fields, the energy spectrum is described by the Kolmogorov spectrum $k^{-5/3}$ (regime of classical Kolmogorov turbulence, Kolmogorov 1941, hereafter K41). It was found that the observed (Matthaeus et al. 1982) and simulated (Pouquet et al. 1988; Politano et al. 1989) energy spectrum of solar wind plasma is close to $k^{-5/3}$.

In the MHD case, Alfven effect (Biskamp 1993) may take place, when small-scale fluctuations are influenced by the large-scale magnetic field. Thus, Iroshnikov (1964) and Kraichnan (1965) found that the Alfven effect may produce an energy spectrum $k^{-3/2}$, when the correlation between velocity and magnetic fields is weak. Consequences of the Alfven effect are still a subject for debates (Biskamp 1993).

In inhomogeneous non-stationary MHD turbulence, a flux tube gets into an environment, where its flux and field strength far exceed the values corresponding to the local turbulent equilibrium. In such situation, turbulent diffusion will dominate over concentration, leading to the slow dissolution of the flux tube (Petrovay & Moreno-Insertis 1997). As a result, the spatio-temporal structure of the energy dissipation becomes burst-like, or intermittent (Biskamp 1993, Frisch 1995). Note, that in MHD, the energy spectrum consists of two components: kinetic energy spectrum and magnetic energy spectrum (which are not necessary identical, Biskamp 1993). The latter, also called as magnetic power spectrum, will be the focus of this study.

Thus, dynamical processes observed in the solar photospheric plasma (emerging of new magnetic flux, decaying of the existing flux, fragmentation and concentration of magnetic elements, etc.) should be reflected in the magnetic power spectrum.

In the past, studies of magnetic power spectra, calculated as the Fourier spectrum of the measured line-of-sight component of the magnetic field, were rather scanty (Nakagawa & Priest 1973; Nakagawa & Levine 1974; Knobloch & Rosner 1981; Lee et al. 1997;

Abramenko et al. 2001). Nakagawa & Priest (1973) obtained power spectra from Kitt Peak longitudinal magnetograms of typical active and quiet regions with a spatial resolution of 2.5 arcsec and reported that on spatial scales $r > 10$ Mm the active region spectrum behaves as $\sim k^{-1}$, while the quiet sun spectrum is described by $k^{-0.3}$. Later, using high resolution Big Bear Solar Observatory (BBSO) videomagnetograms with a spatial resolution of 1.2 arcsec, Lee et al. (1997) calculated the magnetic power spectrum for a quiet region. Authors report that at scales $r > 2$ Mm the spectra can be fitted by k^{-1} while at smaller scales the spectrum behaves as $\sim k^{-3.7}$. Abramenko et al. (2001) calculated magnetic power spectra in the scale range $(3 - 10)$ Mm for one active and one quiet region by using BBSO (Spirock et al. 2001) and Michelson Doppler Imager (MDI, Scherrer et al. 1995) instruments and they found a nearly Kolmogorov spectrum for an active region and a spectrum with the power index of -1.3 for a quiet sun area.

To our knowledge, neither comparison of power spectra calculated for different active regions, nor time evolution of power spectrum in a single active region, have been done as of now. Here we present results of calculation of magnetic power spectra from the photospheric line-of-site magnetograms for 16 active regions. Magnetographic data for three of them allowed us to to calculate the time variations of the power spectrum. For all active regions, we compared the power index of the spectrum with the daily soft X-ray (SXR) flare index (Antalova 1996) calculated for a given active region.

2. Calculation of the Power Spectrum

A spectrum of energy of a 2D real function $u(\vec{l})$ is defined as (Monin and Yaglom 1975):

$$F(\vec{k}) = |U(\vec{k})|^2, \tag{1}$$

where $U(\vec{k})$ is the Fourier transform (FT) of $u(\vec{l})$ and $\vec{k}$ is a wave vector. In our case $u(\vec{l})$ is the line-of-sight component of the photospheric magnetic field, $B_{||}$, measured on a plane (x, y) (a magnetogram) in a rectangular mesh ω:

$$\omega : (x_i = i \cdot \Delta x, i = 1, ..., N_x; y_j = j \cdot \Delta y, j = 1, ..., N_y) \tag{2}$$

with the pixel size defined as $(\Delta x, \Delta y)$.

Then $U(\vec{k})$ are complex numbers specified on a grid Ω:

$$\Omega : \left(k_{x,i} = i \cdot \Delta k_x, i = -\left(\frac{N_x}{2} - 1\right), ..., \frac{N_x}{2}; k_{y,j} = j \cdot \Delta k_y, j = -\left(\frac{N_y}{2} - 1\right), ..., \frac{N_y}{2}\right), \tag{3}$$

with the zero wavenumber at the origin and

$$\Delta k_x = 2\pi/(N_x \Delta x) \text{ and } \Delta k_y = 2\pi/(N_y \Delta y). \tag{4}$$

Thus, a square of the Fourier transform of the field $u(\vec{l})$ provides a 2D power spectrum $F(k_x, k_y)$ defined on the 2D mesh Ω. In order to obtain a one-dimensional power spectrum denoted as $E(k)$ with $k = \sqrt{k_x^2 + k_y^2}$, one has to integrate $F(k_x, k_y)$ in the wavenumber space along the circles $k = |\vec{k}|$ (Monin and Yaglom 1975):

$$E(k) = \int_{|\vec{k}|=k} F(\vec{k}) \cdot dS(\vec{k}). \tag{5}$$

Here $dS(\vec{k})$ is an element of the length of circle $|\vec{k}| = k$. Then, on the mesh Ω, Equation (5) can be written as

$$E(k_i) = \Delta S \sum_{k_i - \Delta k/2 \leq |\vec{k}| \leq k_i + \Delta k/2} F(k_x, k_y). \tag{6}$$

where the sum is taken over nodal points of Ω inside the annulus enclosed by two circles of radii $k_i - \Delta k/2$ and $k_i + \Delta k/2$. Equation (6) contains two unknown parameters: the spacing along the one-dimensional wavenumber axis, Δk, and the spacing along each circle, ΔS. The relation between them can be easily found when we equate the total magnetic energy in a unit layer over the entire magnetogram to the total (over the area of a magnetogram) magnetic energy summed over the power spectrum:

$$\frac{1}{8\pi} \sum_{\omega} B_{||}^2 \Delta x \Delta y = A_{mag} \sum_{\Omega} F(k_x, k_y) \Delta k_x \Delta k_y \approx A_{mag} \sum (\sum F(k_x, k_y) \Delta S) \Delta k). \tag{7}$$

Here the inner sum in the right-hand part of second equality is taken over each annulus between two circles of radii $k_i - \Delta k/2$ and $k_i + \Delta k/2$ and the outer sum is taken over all annuluses which are centered in the origin of Ω and can be inscribed into the Ω (the width of each annulus is Δk). A_{mag} is the area of a magnetogram in the same units as $\Delta x \Delta y$ in the left side part of Equation (7). The second equality in Equation (7) is approximate because of the outer Ω's corners of very low density (the most part of power is always concentrated in the vicinity of the origin of Ω, at low wavenumbers) are not enclosed by the largest annulus that can be inscribed into the Ω. Thus, the relation follows:

$$\Delta S = 1/(8\pi \Delta k). \tag{8}$$

Now, one has to specify only one parameter, Δk. Let us determine it as:

$$\Delta k = p\sqrt{\Delta k_x^2 + \Delta k_y^2}, \tag{9}$$

where p is the width of each annulus in units of the diagonal of a cell in the wavenumber space. The magnitude of p does not change the slope of the calculated spectrum, however,

it affects the spectral resolution. Thus, when $p < 1$ the spectrum has efficient resolution but it is strongly jagged and when $p > 2$ the spectrum is smooth enough but the spectral resolution is low. In the present study, the magnitude of p was adopted specific for each active region (between 1.15 and 1.40) so that the difference between the left and the right parts in Equation (7) was minimal.

The power index of the spectrum, $E(k) \sim k^{-\alpha}$, is defined as a slope of $E(k)$ versus k in a double logarithmic plot within an inertial range: $k_{in} < k < k_d$. Here k_{in} represents the energy injection range, i.e. the large scales, where turbulence excitation occurs and which carry the most of turbulence energy and k_d corresponds to the dissipation scales, i.e. the smallest scales present in the turbulence. For active regions magnetograms, k_{in} is $20 - 100$ Mm and k_d is of order of 0.1 Mm. The determination of the power index α inside the inertial range is the main subject of the present study.

3. Observational Data

In this study we analyzed line-of-sight magnetograms obtained for 16 active regions (Table 1) in high resolution (HR) mode by the Michelson Doppler Imager (MDI) instrument (Scherrer et al., 1995) onboard the Solar and Heliospheric Observatory (SOHO). The data were recorded in the Ni I 6768Å spectral line with a 94 mÅ bandpass filter with spatial resolution of 1.25 arcsec and the corresponding pixel size of 0.58×0.58 arcsec. The detection limit for the magnetic flux density is approximately 17 G (Schrijver et al. 1997). All magnetograms were located near the center of the solar disk, so that the projection effect is negligible, thus, the line-of-sight components of the magnetic field is below denoted as B_z.

Active regions analyzed in the present study had different sizes. The averaged from 16 active regions size of the field-of-view amounts to $N_x \times N_y = 400 \pm 70 \times 270 \pm 40$ pixels, which gave us the averaged number of data points along the spectrum $n_k = 86 \pm 15$. The maximum and minimum scales presented in the spectrum amount to $l_{max} = 150 \pm 30$ Mm and $l_{min} = 0.89 \pm 0.005$ Mm, respectively.

For three active regions NOAA AR 9077, 0365 and 0061, we analyzed long time series of magnetograms. Thus, for NOAA AR 9077, 309 magnetograms obtained on July 13 between 17:10 UT and 23:38 UT and 250 magnetograms obtained on July 14, 2000 between 6:15 UT and 10:47 UT were analyzed. There were 429 magnetograms for NOAA AR 0061 obtained on August 9, 2002 between 11:06 UT and 18:59 UT. The time cadence was 1 minute for both active regions. Due to a large data set for NOAA AR 0365, we analyzed

Table 1: List of studied active regions and calculated parameters

NOAA AR and magnetic type	Period of observations	N[a]	Strongest Flare, X-ray class	Flare Index, A	Power index $\alpha, (3-10)$Mm	Power index $\alpha, (2-20)$Mm
0375 (emerging $\beta\gamma\delta$)	Jun 6-8, 2003	13	X1.7	130.6	2.311 ± 0.070	2.329 ± 0.104
9077 (stable $\beta\gamma\delta$)	Jul 13-14, 2000	559	X5.7	119.9	2.263 ± 0.126	2.281 ± 0.150
0365 (emerging $\beta\gamma\delta$)	May 25-27, 2003	520	X3.6	104.4	2.136 ± 0.082	2.133 ± 0.090
0488 (emerging $\beta\gamma\delta$)	Oct 29, 2003	2	X3.9	91.8	2.216 ± 0.030	2.211 ± 0.027
0030 (emerging $\beta\gamma\delta$)	Jul 15-16, 2002	8	X3.0	59.3	2.166 ± 0.068	2.187 ± 0.045
0501 (stable $\beta\gamma\delta$)	Nov 18-19, 2003	12	M9.6	39.5	2.005 ± 0.055	2.058 ± 0.114
9661 (stable $\beta\gamma\delta$)	Oct 16-17, 2001	7	X1.6	33.5	2.093 ± 0.032	2.112 ± 0.026
9773 (emerging $\beta\gamma\delta$)	Jan 8-9, 2002	6	M9.5	23.4	2.036 ± 0.108	2.049 ± 0.061
0134 (stable $\beta\gamma\delta$)	Sep 30-Oct 1, 2002	5	M2.6	18.2	1.915 ± 0.055	1.974 ± 0.039
8375 (stable $\beta\gamma$)	Nov 4-5, 1998	6	M2.7	17.0	1.812 ± 0.140	1.822 ± 0.097
9866 (stable $\beta\delta$)	Mar 14-15, 2002	9	M5.7	13.1	2.051 ± 0.105	2.059 ± 0.028
0149 (stable $\beta\gamma$)	Oct 14-16, 2002	18	M1.0	3.8	1.811 ± 0.078	1.843 ± 0.043
0061 (stable $\beta\gamma$)	Aug 9, 2002	429	C3.3	2.6	1.668 ± 0.060	1.768 ± 0.022
0306 (stable $\beta\gamma$)	Mar 13-14, 2003	3	C2.6	0.4	1.780 ± 0.044	1.816 ± 0.024
9851 (emerging β)	Mar 6, 2002	4	-	0.0	1.737 ± 0.035	1.733 ± 0.020
0515 (decay β)	Dec 3, 2003	2	-	0.0	1.627 ± 0.040	1.635 ± 0.023

[a]− number of analyzed magnetograms.

520 magnetograms with the 5-minute cadence obtained during 3 days, between 10:01 UT on May 25, 2003 and 9:59 UT on May 27, 2003. Unfortunately, MDI HR observations, available for the rest of active regions, allowed us to analyze only few magnetograms for each active region. The number of magnetograms used for each active region is noted in the 3rd column of Table 1. The strongest flare occurred in a given active region during its passage across the solar disk is presented in the 4th column of Table 1.

To quantify the flare productivity of a given active region we used the daily SXR flare index that was first introduced by Antalova (1996) and was later applied by other authors (e.g., Landi et al. 1998, Joshi and Joshi 2004) to characterize the daily flare productivity of the Sun from the soft X-ray flux measured by GOES satellite in the 1-8Årange. We calculated this index for each active region selecting the X-ray peaks associated with a given active region.

The X-ray classification of solar flares (X, M, C, B classes) is based on the denary logarithmic scale. This allowed Antalova (1996) to define the flare index by weighing the SXR flares of classes B, C, M and X as 0.1, 1, 10 and 100 respectively (in units of 10^{-6} Wm−2) regardless the duration of the flare. Then, the daily SXR flare index can be written

as (Pevtsov 2004, Longcope 2005):

$$A = (100S^{(X)} + 10S^{(M)} + 1.0S^{(C)} + 0.1S^{(B)})/\tau, \tag{10}$$

where $S^{(j)} = \sum_{i=1}^{N_j} I_i^{(j)}$ is the sum of GOES peak intensities of a certain class (in other words, the digits from 1.0 to 9.9 following the letters X, M, C, B). $N_j = N_X, N_M, N_C$ and N_B are the numbers of flares of X, M, C and B classes, respectively, that occurred in a given active region during the time interval τ (measured in days) between the moment when the active region was first observed in the SOHO MDI full disk images and the moment when it was observed for the last time. The accuracy of determination of τ is no better than ± 0.5 days. Thus, $A = 1$ corresponds to a specific flare productivity of one flare of C1.0 class per day. It is worth noting, however, that the above definition should be used with caution when long duration SXR events are considered (Antalova and Viktorinova 1991, Landi et al. 1998).

The daily SXR flare index calculated from Equation (10) for a given active region is referred hereinafter as the flare index. Flare indices calculated for each active region are presented in the 5th column of Table 1. The active regions in Table 1 are arranged in accordance with the decrease of the flare index A.

4. Magnetic Power Spectra

For each longitudinal magnetogram, available for the active regions listed in Table 1, we calculated a power spectrum.

A range of scales, where determination of the power index is the most reliable, was determined in our previous study (Abramenko et al 2001). It was shown that when the power index is calculated over the scales $r > 3$ Mm (for SOHO MDI high resolution magnetograms) the result is marginally affected by the influence of noise and insufficient resolution of the telescope. We corrected the spectrum for the insufficient resolution by the modulation transfer function (Abramenko et al. 2001) and observed the extension of the linear range of the spectrum with the same slope beyond 3 Mm, which may indicate that the real inertial range extends towards scales smaller than 3 Mm. We made a conclusion that the observed smooth cutoff of the spectrum at scales $r \approx 3$ Mm is caused by the insufficient resolution of the data. Therefore, the best way to calculate the power index from uncorrected spectra is to specify the high-wavenumber end of the linear range at 3 Mm, which was done in the present study.

At the low-wavenumber end of the spectrum, large sunspots may contribute significantly in the power at scales of about $20 - 40$ Mm. However, they might not belong to the inertial range of turbulence but rather to the energy injection range. Abramenko et al. (2001)

calculated the power spectrum over a magnetogram with blocked large spot and compared it with the power spectrum from the original magnetogram. Comparison showed that at scales $r < 10$ Mm the influence of large spots at the spectrum is negligible.

The above considerations allowed us to specify the range $\Delta r = (3 - 10)$ Mm as the part of a *real* inertial range where the spectrum slope will reflect the real power index in the best way possible under the current accuracy of magnetographic measurements. Although observed magnetic spectra of active regions (see Figures 1, 3, 5 and 6) demonstrate linearity in a range wider than $(3 - 10)$ Mm, this interval was used as the most reliable one. The power indices in this range (determined for each active region by averaging over all magnetograms) are presented in 6-th column of Table 1. A wider interval $(2 - 20)$ Mm was tried in parallel and the corresponding power indices are presented in the 7-th column of Table 1. The comparison of these two columns shows that the choice of Δr is not crucial for the calculation of the power index: the wide range produces practically the same slope as the narrow range. Note, however, that the wide range gives consistently slightly higher magnitude of α than the narrow range does, which is related to the high-wavenumber cutoff of the spectra at scales $r < 3$ Mm.

Magnetograms and the corresponding power spectra calculated for NOAA AR 9077 are shown in Figure 1. The comparison of the two magnetograms obtained on July 13 and 14 shows that this active region evolved rapidly and displacement and fragmentation of large-scale concentrations of the magnetic flux can be noticed in the data. The observed power spectra (*right panel* in Figure 1) are significantly steeper than the Kolmogorov spectrum $k^{-5/3}$ (the dashed line).

Time variations of the power index α (Figure 2) show undulating changes of no significant correlation with the GOES $1 - 8$Å X-ray flux. The magnitude of α slightly decreased from July 13 to July 14, nevertheless it still significantly exceeded the Kolmogorov value of $5/3$, as well as the Iroshnikov-Kraichnan value of $3/2$. It is worth noting here that NOAA AR 9077 was a magnetic structure of very high flare productivity: during the passage across the solar disk, it launched 37 flares of X-ray class higher than C3, among them thirteen M-class flares and three X-class flares.

Figure 3 shows MDI data and power spectra for an emerging and very flare productive active region NOAA AR 0365. At the very beginning of the emergence this magnetic region displayed a very steep non-Kolmogorov spectrum $k^{-2.2}$. Visual inspection of the three magnetograms in Figure 3 shows that the emergence of new magnetic flux in this active region led to increase of power at all wavenumbers lifting the spectrum up with nearly the same slope (see *right panel* in Figure 3). Figure 4 shows time variations of the power index and of the flare activity in the same active region. One may conclude from this figure that
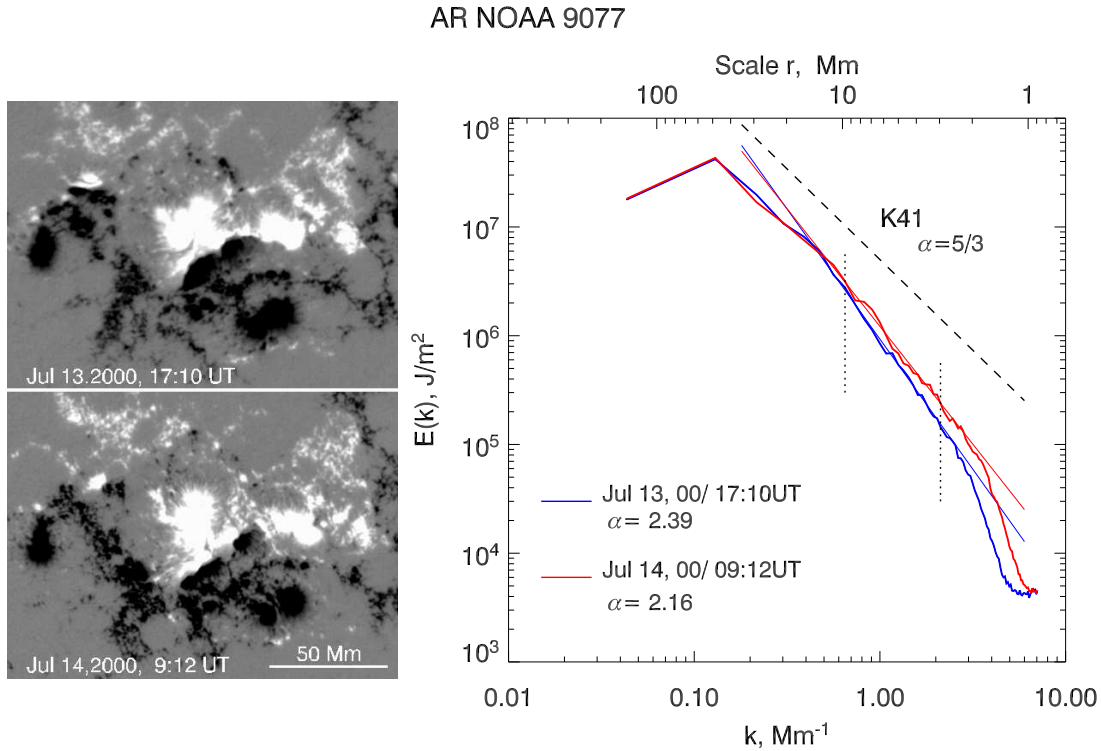
Fig. 1.— *Left* - MDI high resolution line-of-sight magnetograms for NOAA active region 9077. *Right* - Power spectra calculated from the magnetograms showed. The thin straight lines show linear best fits to the observed spectra in the range of scales $\Delta r = (3 - 10)$ Mm (indicated by vertical dotted segments). State of Kolmogorov turbulence, $\alpha = 5/3$, is shown by the dashed line.

during this three-day observation period the magnetic power spectrum was significantly steeper than the Kolmogorov spectrum $k^{-5/3}$ and that the magnitude of α slightly decreased (from 2.3 to 2.0).

Other emerging active regions analyzed in the present study showed the similar result, which is summarized in Table 2. The third column shows the time of the first magnetogram in the data set. Fortunately, for all emerging active regions, the first magnetogram was obtained *before* the beginning of intensive flare activity, i.e. before the strongest flares occurred in a given active region. The 4-th column represents the power index calculated from the first magnetogram. The last column shows the averaged (over all analyzed magnetograms in the data set) power index $< \alpha >$, which is the same as 6-th column of
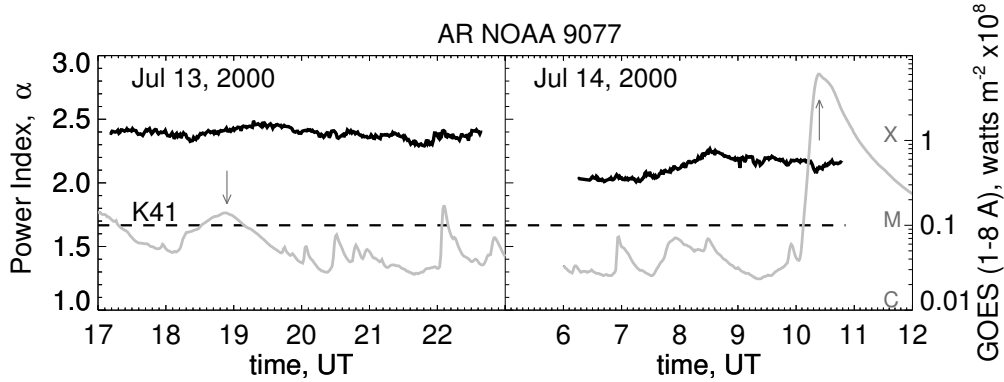
Fig. 2.— Time variations of the power index calculated for active region NOAA 9077 (left axis is valid for both panels). State of Kolmogorov turbulence is shown by *black dashed line*. GOES 1-8Å X-ray flux (right axis) is shown by *gray lines*. The arrows mark the X-ray flux peaks related to flares occurred in the active region under study.

Table 1. The comparison between the two last columns of Table 2 demonstrates that the power index at the beginning of the emergence (before the flare activity) was very similar to the averaged power index. Moreover, the steeper the spectrum at the beginning of the emergence the higher the future flare productivity. Thus, when an active region emerges with the power index close to 5/3 it is prone to display a very low flare activity, as NOAA AR 9851 demonstrated (see the bottom line in Table 2 and Figure 5.)

Table 2: List of emerging active regions and calculated parameters

NOAA AR	Flare Index, A	Time of the first magnetogram	α from the first magnetogram [a]	$< \alpha >$ [a,b]
0375	130.6	Jun 6, 2003, 20:26 UT	2.22	2.31
0365	104.4	May 25, 2003, 10:01 UT	2.23	2.14
0488	91.8	Oct 29, 2003, 15:47 UT	2.22	2.22
0030	59.3	Jul 15, 2002, 10:54 UT	2.20	2.17
9773	23.4	Jan 8, 2002, 20:23 UT	1.94	2.04
9851	0.0	Mar 6, 2002, 10:13 UT	1.74	1.74

[a]— the power index α was calculated over the $(3 - 10)$ Mm range of scales.
[b]— $< \alpha >$ is the power index averaged over all analyzed magnetograms as it is presented in the 6-th column of Table 1.

Magnetograms and power spectra for a stable and flare-quiet active region NOAA 0061 are shown in Figure 6. An eight-hour movie of this active region showed that main evolutionary changes in this active region consisted of random motions, fragmentation
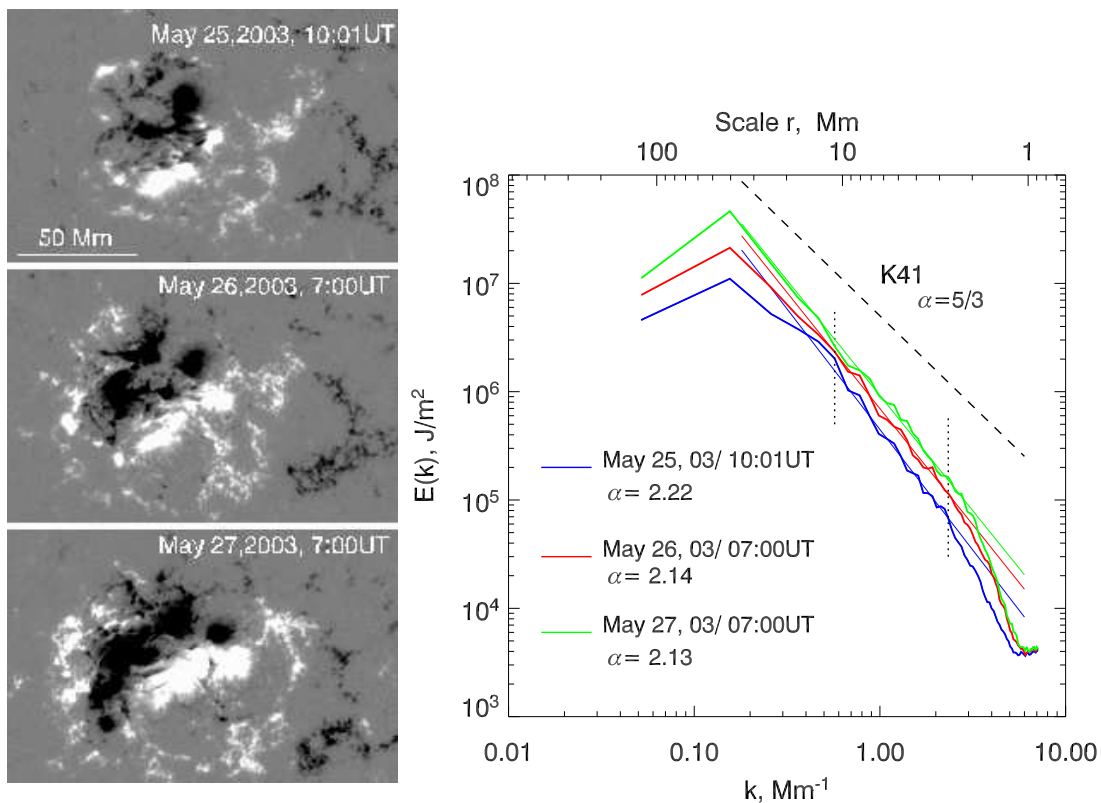
Fig. 3.— *Left* - MDI high resolution line-of-sight magnetograms for the emerging and flare productive active region NOAA 0365. *Right* - Power spectra calculated from the magnetograms showed in the left panels. Notations are the same as in Figure 1.

and/or merging of small scale magnetic elements everywhere outside the main spot. Around the main spot, regular radial moat outflows of magnetic elements erosioning the spot dominated. The power spectrum for this active region is very close to the Kolmogorov spectrum (see *right panel* in Figure 6) with the power index α fluctuating around the K41 line (Figure 7).

Results from three active regions with extended data sets suggest that the power index α of the magnetic power spectrum does not changes drastically during several days. This allowed us to consider the magnitude of α, derived from a few magnetograms, as a representative estimation of the power index for a given active region.

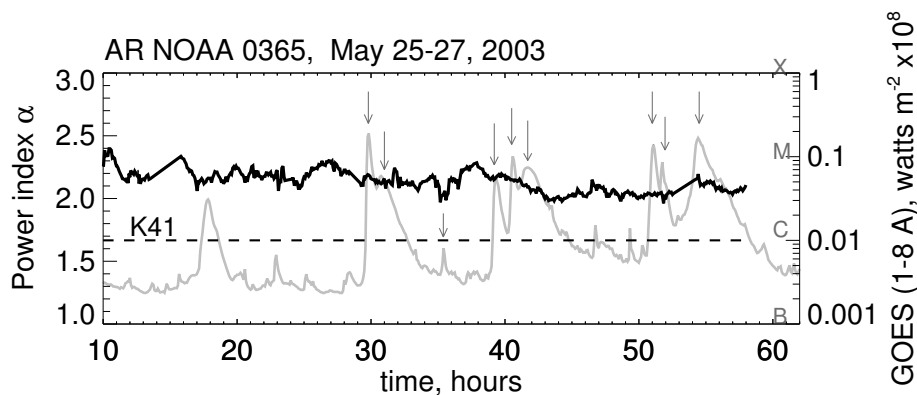Thus, Figure 8 summarizes results obtained for 16 active regions. In the figure we plot

Fig. 4.— Time variations of the power index α calculated for the emerging and flare productive active region NOAA 0365 and 1-8Å X-ray GOES flux. Notations are the same as in Figure 2.
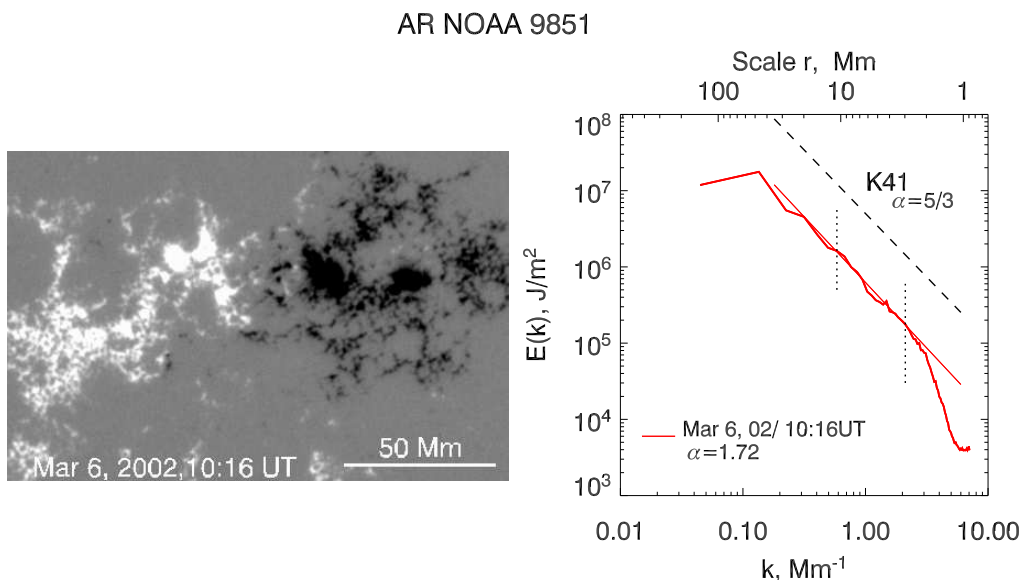

Fig. 5.— *Left* - MDI high resolution line-of-sight magnetogram of an emerging non-flaring active region NOAA 9851. *Right* - Power spectrum calculated from the magnetogram showed on the left panel. Notations are the same as in Figure 1.

the magnitude of the power index, α, of a given active region versus its flare index A. For $\alpha > 5/3$, the best fit to the observed data can be represented with an analytical curve

$$A(\alpha) = C(\alpha - 5/3)^n, \tag{11}$$

with $C = 409.5 \pm 6.3$, $n = 2.49 \pm 0.025$ and the reduced $\chi^2 = 1.07$. Thus, our results show a strong correlation between the flare index, A, and the magnitude of the power index, α.
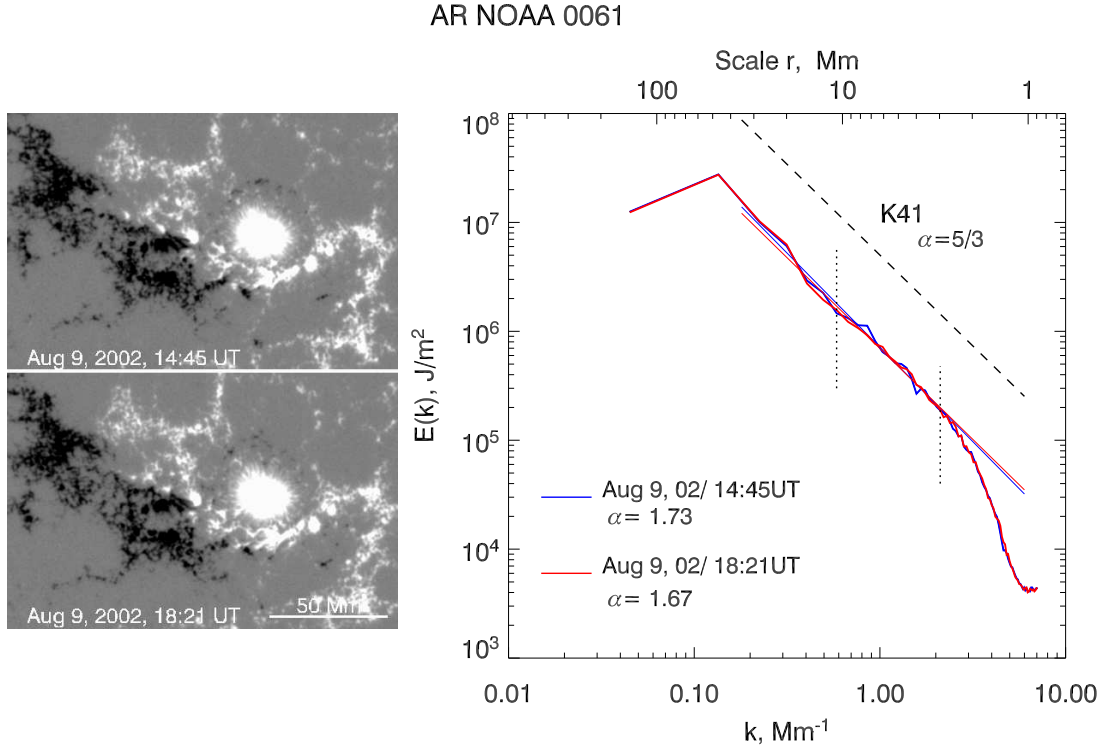
Fig. 6.— *Left* - MDI high resolution line-of-sight magnetograms of a stable non-flaring active region NOAA 0061. *Right* - Power spectra calculated from the magnetograms showed on the left panels. Notations are the same as in Figure 1.
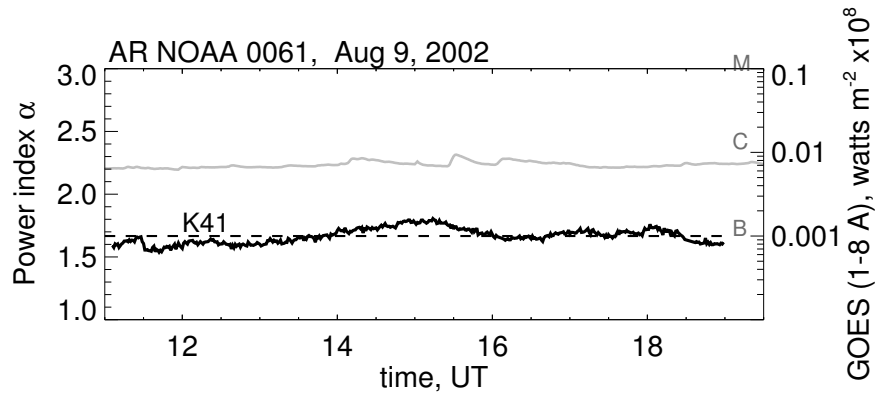

Fig. 7.— Time variations of the power index α and the X-ray 1-8Å X-ray GOES flux for active region NOAA 0061. Notations are the same as in Figure 2.

Those active regions which can produce X-class flares, possess very steep power spectrum with $\alpha > 2$, while quiet, non-flaring active regions display Kolmogorov-type spectrum with $\alpha \approx 5/3$. None of analyzed active regions showed the Iroshnikov-Kraichnan spectrum of $\alpha = 3/2$.
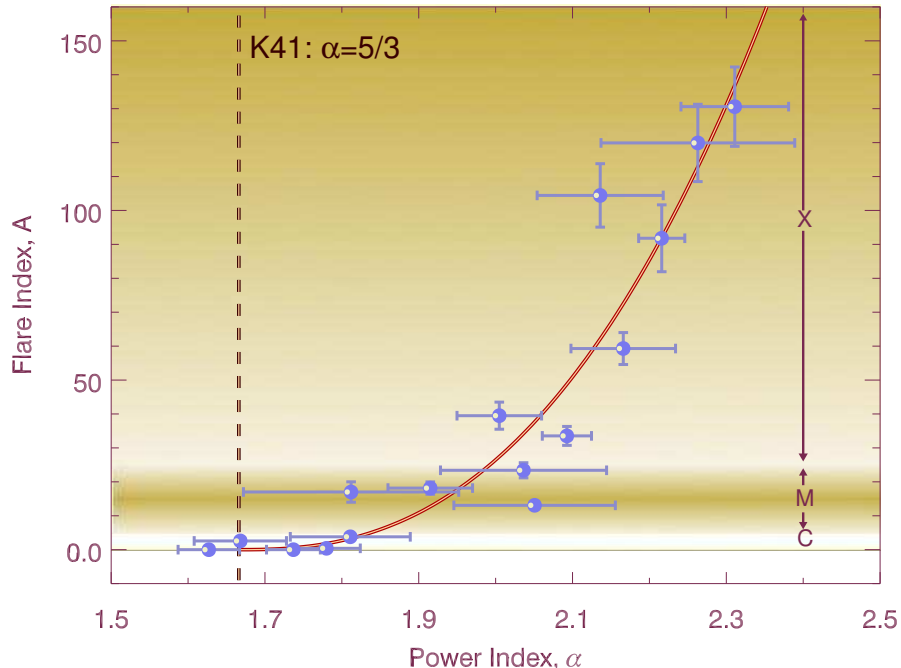

Fig. 8.— Power index α versus flare index A plotted for 16 active regions listed in Table 1. The dashed straight line indicates the power index $\alpha = 5/3$ for the stationary classical Kolmogorov turbulence K41. The curve shows the best fit $A(\alpha) = 409.5(\alpha - 5/3)^{2.49}$ to the data.

It is worth noting that for NOAA AR 8375, the magnetic power spectrum was analyzed in our previous study (Abramenko et al. 2001). Only one high resolution MDI magnetogram obtained on November 4, 1998 was used and the power index of approximately -1.7 was reported. In the present study we used 6 high resolution MDI magnetograms for this active region. Three of them were obtained on November 4, 1998 and they showed the Kolmogorov-type spectrum (in accordance with Abramenko et al. 2001), whereas the rest of them, obtained on November 5, 1998, displayed a steeper spectrum of $k^{-1.9}$. This resulted in the averaged value of $\alpha = 1.81$ and large error bars (see Table 1).

5.   Conclusions

In order to learn more about the turbulent state of the photospheric plasma, we calculated a power spectrum of the magnetic field. Sixteen active regions of different flaring activity were analyzed by using line-of-sight SOHO/MDI high resolution magnetograms. We compared the power index, α, of the spectrum with the daily SXR flare index, A, of a given active region. The value of A characterizes the flare productivity of an active region per day.

The present study demonstrates that higher flare productivity seems to be associated with a steeper magnetic power spectrum, $E(k) \sim k^{-\alpha}$. Active regions which produced X-class flares, possessed a steep power spectrum with $\alpha > 2.0$. On the other hand, flare-quiet active regions with low flare index A displayed a Kolmogorov-type spectrum of $\alpha \approx 5/3$. Observational data suggest that the flare index A may be determined from the power index α by $A(\alpha) = 409.5(\alpha - 5/3)^{2.49}$.

Also noteworthy is that the magnitude of the power index, determined during the emergence of an active region, seems not to be related to its current flare productivity. Instead, an emerging magnetic structure that displays a very steep ($\alpha > 2$) magnetic power spectrum is prone to produce X-class flares in the future. This finding shows the way to distinguish at the very early stage those solar spots that are "born bad" and have a potential to produce significant disturbances in the earth magnetosphere.

The above result may suggest that the turbulence state of flaring and quiet active regions is different, which may partially explain the different level of flare activity. The very steep non-Kolmogorov spectra of flaring active regions imply the inhomogeneous non-stationary turbulence regime when the energy transport rate along the spectrum may not be constant. Then, the energy dissipation displays an intermittent behavior as in time so in spatial domains (Frisch 1995, Biskamp 1993). On the other hand, the Kolmogorov-type spectra of quiet active regions might suggest a nearly stationary turbulent regime with constant rate of energy transfer along the spectrum. In this case, dynamical equilibrium between the input of energy at large scales and output at small scales provides premises for smooth evolution without catastrophes.

This study has demonstrated that structural and dynamical characteristics of the magnetic field as measured in the photosphere are relevant to the intensity of non-stationary processes in the entire magnetic configuration.

REFERENCES

Abramenko, V.I., Yurchyshyn, V.B., Wang, H., Goode, P.R. 2001, Solar Phys., 201, 225

Antalova, A. 1996, Contributions of the Astronomical Observatory Skalnate Pleso, 26, 98.

Antalova, A., Viktorinova, B., 1991, Bull. Astron.Inst. Czechosl., 42, 133.

Biskamp, D. 1993, "Nonlinear Magnetohydrodynamics", Cambridge University Press, New York, 378 pp.

Frisch, U. 1995, "Turbulence, The Legacy of A.N. Kolmogorov", Cambridge University Press

Iroshnikov, P.S. 1964, Sov. Astron., 7, 566-71.

Joshi, B., Joshi, A. 2004, Solar Phys. 219, 343.

Knobloch, E., Rosner, R. 1981, ApJ, 247, 300.

Kolmogorov, A.N. 1941, C.R. Acad. Sci. USSR, 30, 301.

Kraichnan, R.H. 1965, Phys. Fluids 8, 1385-7.

Landi, R., Moreno, G., Storini, M., Antalova, A. Journal of Geoph. Res. 103, NO. A9, p. 20,553

Lee, J.W., Chae, J.C., Yun, H.S., Zirin, H. 1997, Solar Phys., 171, 269.

Longcope, D.W.: 2005, *private communication.*

Matthaeus, W.H., Goldstein, M.L., Smith, C. 1982, Phys. Rev. Lett. 48, 1256-9

Monin, A.S., Yaglom, A.M. 1975, "Statistical Fluid Mechanics", vol. 2, ed. J.Lumley, MIT Press, Cambridge, MA

Nakagawa, Y., Prist, E.R. 1973, ApJ, 179, 949.

Nakagawa, Y., Levine, R.H. 1974, ApJ, 190, 441.

Parker, E.N. "Cosmical magnetic fields, their origin and their activity", Oxford University Press, 1979.

Petrovay, K., Szakaly, G. 1993, Astron. Astrophys., 274, 543.

Petrovay, K. & Moreno-Insertis, F., ApJ, 485, 398

Pevtsov, A.A.: 2004, *private communication.*

Politano, H., Pouquet, A., Sulem, P.L. 1989, Phys. Fluids 31, 2330-9.

Pouquet, A., Sulem, P.L., Meneguzzi, M. 1988, Phys. Fluids 31, 2635-43

Schrijver, C.J., Title, A.M., Hagenaar, H.J., Shine, R.A. 1997, Solar Phys., 175, 329

Scherrer, P.H., Bogart, R.S., Bush, R.I., Hoeksema, J.T., Kosovichev, A.G., Schou, J., Rosenberg, W., Springer, L., Tarbell, T.D., Title, A., Wolfson, C.J., Zayer, I. and the MDI engineering team, 1995, Solar Phys., 162,129.

Spirock, T.J., Denker, C., Chen, H., Chae, J., Qiu, J., Varsik, J., Wang, H., Goode, P.R., Marquette, W.: 2001, in *Advanced Solar Polarimetry Theory, Observation, and Instrumentation*, ed. M. Sigwarth (ASP-236; San Francisco: ASP) , 65

Spruit, H.C. 1981, in *The Sun as a Star* edited by S. Jordan (NASA, Washington , D.Cc.), NASA Monograph Series SP-45

Stenflo, J.O., Holzreuter, R. 2002, in: SOLMAG 2002, ESA SP-505, 101